Journal of Materials Chemistry A

RSC Publishing

PAPER

View Article Online
View Journal | View Issue

Cite this: J. Mater. Chem. A, 2013, 1, 7154

Synthesis of α-Fe_2O_3 nanoparticles from $Fe(OH)_3$ sol and their composite with reduced graphene oxide for lithium ion batteries†

Meng Du, Chaohe Xu, Jing Sun* and Lian Gao

Received 13th January 2013
Accepted 5th April 2013

DOI: 10.1039/c3ta00183k

www.rsc.org/MaterialsA

α-Fe_2O_3/reduced graphene oxide (α-Fe_2O_3/RGO) composite has been synthesized by a facile hydrothermal method. $Fe(OH)_3$ sol is creatively employed as the precursor and no nucleating agent is employed to help Fe^{3+} change to $Fe(OH)_3$. In the hydrothermal process, $Fe(OH)_3$ sol transforms to α-Fe_2O_3 particles and GO becomes RGO with hydrazine hydrate. Composites with different ratios between α-Fe_2O_3 and RGO for comparison are investigated as anode LIB materials. Among the composites, the α-Fe_2O_3/RGO containing 73% α-Fe_2O_3 exhibits the highest reversible specific capacity of ~950 mA h g^{-1} after 70 cycles at a current density of 100 mA g^{-1}. When the current density is 800 mA g^{-1}, the capacity still remains as ~700 mA h g^{-1}, showing superior rate capability. The significant electrochemical property improvements of α-Fe_2O_3/RGO can be attributed to the uniform α-Fe_2O_3 nanoparticles (20–30 nm) and the RGO substrate, which provides high electrical conductivity and stability.

1 Introduction

Rechargeable LIBs as an important kind of power source have been greatly used for popular consumer electronics. They are also considered as the most promising batteries for hybrid electric vehicles.[1,2] In order to meet the increasing demand for higher reversible capacities, metal oxides, such as SnO_2, Fe_2O_3, Fe_3O_4, Co_3O_4 and Mn_3O_4,[3–7] are widely studied for their higher reversible capacity than commercial graphite (372 mA h g^{-1}). Among them α-Fe_2O_3 has the highest theoretical capacity of 1005 mA h g^{-1}. Moreover, its low cost, eco-friendliness and elemental abundance have attracted considerable attention.[8,9] However, the severe aggregation and huge volume change of α-Fe_2O_3 particles during the Li insertion/extraction process may cause the pulverization of the electrodes, leading to poor cycling performance.[10] Recently, α-Fe_2O_3 materials with various nanostructures, such as nanocubes, nanocapsules, nanorods and so on,[8,11,12] have been employed to improve the reversible capacity and cycling performance. For example, Koo *et al.*[13] designed different Fe_2O_3 morphologies and studied the relationship between the morphology and electrical properties. They showed that hollow Fe_2O_3 nanoparticles could reach up to 1228 mA h g^{-1}, however, the reversible capacity reduced to about 200 mA h g^{-1} after cycling 15 times. Chen *et al.*[14] demonstrated a facile top-down approach to fabricate uniform single-crystal α-Fe_2O_3 nanodiscs, which showed 662 mA h g^{-1} at a current rate of 200 mA g^{-1} after 100 charge–discharge cycles. Another strategy to enhance the cycling ability was by coating carbon on metal oxide,[15] while the conductivity of the composites did not improve a lot and it just delayed the pulverization of the metal oxide anodes to some degree. Over extended cycling, poor capacity retention would still appear unfortunately.

Graphene, with its high conductivity and large specific surface area, as well as flexibility and chemical stability, is an excellent substrate to hybridise with active nanomaterials for energy applications.[16,17] More and more metal oxide/graphene composites are synthesized as enhanced LIB anodes.[18,19] In addition, graphene as an outstanding host conductor could make up for the weak electrical conductivity of metal oxides. Besides, the flexible thin graphene film will absorb the stress produced in the Li insertion/extraction process. The metal oxide/graphene hybrids can not only keep a high reversible capacity, but also reveal enhanced cycling performance.[20–22] Bai *et al.*[23] utilized a facile solvothermal method to synthesize Fe_2O_3 nanospindles with crumpled RGO nanosheets, revealing a high reversible capacity of 969 mA h g^{-1} after 100 cycles at a current density of 100 mA g^{-1}. Zhu *et al.*[24] prepared an α-Fe_2O_3/RGO composite using a homogeneous precipitation of $FeCl_3$ in a suspension of GO platelets with urea, with subsequent reduction of the GO with hydrazine under microwave irradiation to yield RGO platelets decorated with Fe_2O_3 nanoparticles. Such a composite reached as high as 1027 mA h g^{-1} after 50 cycles at a current density of 100 mA g^{-1}.

Herein, $Fe(OH)_3$ sol is employed to synthesize α-Fe_2O_3 nanoparticles and further combine with RGO as an anode

The State Key Lab of High Performance Ceramics and Superfine Microstructure, Shanghai Institute of Ceramics, Chinese Academy of Sciences, 1295 Dingxi Road, Shanghai 200050, P.R. China. E-mail: jingsun@mail.sic.ac.cn; Fax: +86-21-52413122; Tel: +86-21-52414301

† Electronic supplementary information (ESI) available. See DOI: 10.1039/c3ta00183k

material for high-performance LIBs. In previous work, the source of the metal oxides was metal salt solutions and the morphology of the final product was hard to control. Under the circumstances the particles of the composites often grew to a large size.[25] However, in this work, the $Fe(OH)_3$ sol has a uniform size of 4–5 nm and excellent dispersity, which ensures that the final α-Fe_2O_3 nanoparticles have a small and uniform size. The excellent uniformity and dispersity of α-Fe_2O_3 particles on RGO can be attributed to the characteristics of sol. Composites with different volume ratios between α-Fe_2O_3 and RGO have been prepared. As a result, we find that when the content of α-Fe_2O_3 reaches 73%, the composite shows the best reversible specific capacity of ~950 mA h g^{-1} after 70 cycles at a current density of 100 mA g^{-1}. In addition, the composite reveals an improved rate capability and when the current density is 800 mA g^{-1}, the capacity still remains ~700 mA h g^{-1}. To the best of our knowledge, this is the first time that sol has been used to synthesize a metal oxide/graphene composite. The strategy presents a promising approach for the synthesis of high quality anode materials of LIBs.

2 Experimental section

2.1 Preparation of the α-Fe_2O_3/RGO composite

Preparation of the $Fe(OH)_3$ sol. 6.5 g $FeCl_3$ was dissolved in 20 mL distilled water to get 2 M $FeCl_3$ solution. Then, 0.5 mL of the solution was dropped into 50 mL boiling distilled water. Finally, the water was kept boiling for several minutes to obtain $Fe(OH)_3$ sol.

Preparation of the α-Fe_2O_3/RGO composite. GO was prepared by a modified Hummers method.[26,27] In a typical synthesis, GO solution (1 mg mL^{-1}) was mixed with $Fe(OH)_3$ sol with a volume ratio of 2 : 1. In the process, $Fe(OH)_3$ sol was added into the GO solution dropwise, followed by stirring for 30 min. Next, hydrazine hydrate (85%) was added into the mixture and then after ultrasonication for 30 min, the solution was transferred into a Teflon-lined autoclave and heated at 150 °C for 6 h. Finally, the resulting composites were washed with deionized water several times, and then dried in a vacuum oven at 60 °C for 10 h. The volume ratios between GO solution (1 mg mL^{-1}) and $Fe(OH)_3$ sol were changed to 4 : 1 and 1 : 1 to synthesize the other two α-Fe_2O_3/RGO composites for comparison. According to the TG result of Fig. S1,† three kinds of α-Fe_2O_3/RGO composites were labeled as 33% α-Fe_2O_3/RGO, 73% α-Fe_2O_3/RGO and 81% α-Fe_2O_3/RGO, respectively, based on the content of α-Fe_2O_3 in the composites. Pure α-Fe_2O_3 particles without RGO were also prepared as a control in the same procedure.

2.2 Materials characterization

The phase identification of the three α-Fe_2O_3/RGO composites and α-Fe_2O_3 particles were performed with powder X-ray diffraction pattern (XRD with Cu Kα irradiation). The zeta potential was measured by the tester (Zetaplus) in pure water. Morphological observation was carried out using a transmission electron microscope (TEM, JEM-2100F at 200 kV). Thermogravimetry (TG) analysis was performed by using a STA409/PC simultaneous thermal analyzer (Netzsch, Germany) in air with a temperature range of 50–750 °C. The cyclic voltammetry (CV) data was taken on a PARSTAT 2273 Electrochemical workstation in the range of 3–0 eV. The Nyquist plots were collected on the same workstation.

2.3 Electrochemical measurements

The electrochemical experiments of the three α-Fe_2O_3/RGO composites and pure α-Fe_2O_3 were performed using CR 2025 type coin cells. The test electrodes were prepared by mixing the active materials, acetylene black, and polyvinylidene fluoride (PVDF) binder in a weight ratio of 80 : 10 : 10. After that the mixtures were dissolved in *N*-methyl-2-pyrrolidone (NMP). The electrolyte used was 1 M $LiPF_6$ in a 50 : 50 weight ratio ethylene carbonate (EC) : dimethyl carbonate (DMC) solvent. The cells were assembled in an argon-filled glovebox and galvanostatically discharged and charged using a CT 2001 battery tester.

3 Results and discussion

As shown in Table 1, $Fe(OH)_3$ sol has a positive charge (11.28 mV of Zeta potential) due to its adsorption of Fe^{3+} cations, while the GO solution exhibits a negative charge (−35.56 mV of Zeta potential). When the two mix together, the $Fe(OH)_3$ particles and GO combine with each other under an attractive force. As a result, the zeta potential of the $Fe(OH)_3$/GO hybrid is 1.31 mV.

Fig. 1 exhibits the synthesis process of the composite. The $Fe(OH)_3$ sol is synthesized without a nucleating agent, leading to a small particle size of about 4–5 nm. After that, it combines with the GO solution. During the hydrothermal process, GO is converted into RGO[28] and $Fe(OH)_3$ is transformed into α-Fe_2O_3 particles *in situ* with small particle sizes of 20–30 nm. The huge specific surface area of RGO makes it quite easy to trap Fe_2O_3 nanoparticles[29] and they will combine tightly with the help of van der Waals forces.

Comparing the XRD patterns (Fig. 2) of GO, commercial α-Fe_2O_3 particles and three α-Fe_2O_3/RGO composites, shows the α-Fe_2O_3 particles in the composites are well crystallized, which agrees well with (JCPDS 33-0664).[30,31] GO has been converted to RGO in the hydrothermal process.[28] However, the peak of graphene at ~25° almost overlaps with the main peak of α-Fe_2O_3 (012).[5]

Fig. 3 shows the TEM images of the $Fe(OH)_3$ sol, $Fe(OH)_3$/GO, α-Fe_2O_3 particles and 73% α-Fe_2O_3/RGO composite. The particle size of the $Fe(OH)_3$ sol is 4–5 nm as shown in Fig. 3a. When the particles combine with the GO, they lay uniformly on the GO

Table 1 The zeta potentials of GO, $Fe(OH)_3$ sol and $Fe(OH)_3$/GO

Sample	1st result (mV)	2nd result (mV)	3rd result (mV)	Average result (mV)
GO	−39.16	−31.34	−36.19	−35.56
$Fe(OH)_3$ sol	12.35	10.04	11.44	11.28
$Fe(OH)_3$/GO	1.33	0.47	2.12	1.31

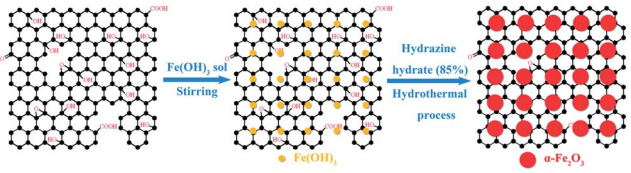

Fig. 1 Schematic diagram for the growth process of the α-Fe_2O_3/RGO composite.

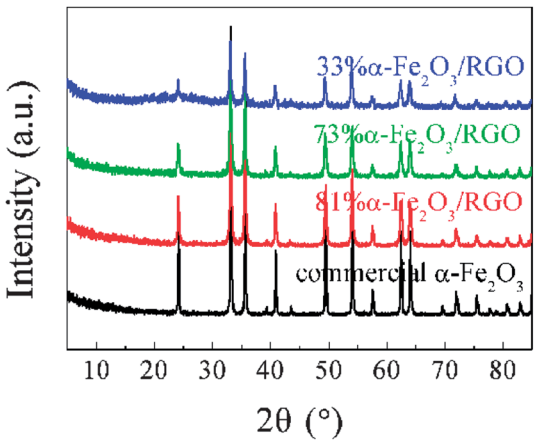

Fig. 2 XRD patterns of α-Fe_2O_3 particles and three α-Fe_2O_3/RGO composites with different ratios of α-Fe_2O_3 and RGO.

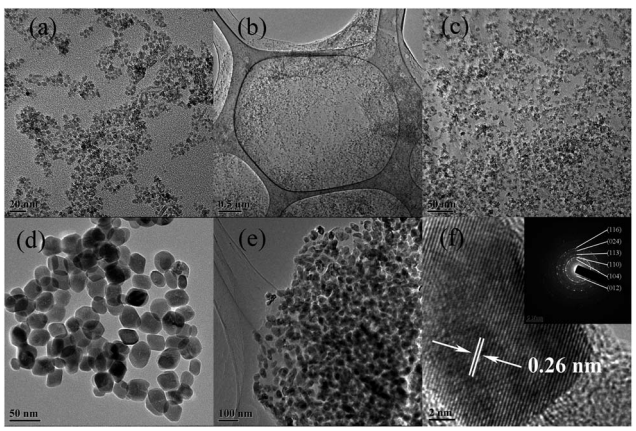

Fig. 3 TEM images of (a) $Fe(OH)_3$ particles, (b and c) $Fe(OH)_3$/GO particles (d) α-Fe_2O_3 particles, (e) 73% α-Fe_2O_3/RGO composite and HRTEM image of (f) 73% α-Fe_2O_3/RGO composite. (Inset) Selected area electron diffraction (SAED) pattern for the 73% α-Fe_2O_3/RGO composite.

layers and the particle size remains unchanged (Fig. 3b and c). The separated α-Fe_2O_3 particles for comparison are shown in Fig. 3d, and the size of the particles is 20–30 nm which remains the same when they combine with RGO. In the 33% α-Fe_2O_3/RGO composite, there are not enough α-Fe_2O_3 particles to fully cover the surface of the RGO (Fig. S2c and d†), as a result, the used ratio of graphene is quite low. The α-Fe_2O_3 particles of the 73% α-Fe_2O_3/RGO composite uniformly decorate the RGO (Fig. 3d). However, in the 81% α-Fe_2O_3/RGO composite there are too many α-Fe_2O_3 particles, and some of them cannot even combine with the graphene (Fig. S2a and b†) and the extra particles group together. So, the 73% α-Fe_2O_3/RGO composite is appropriate for the α-Fe_2O_3 particles to disperse on RGO. Fig. 3f indicates that a lattice spacing of 0.26 nm for the (110) planes clearly identifies the α-Fe_2O_3 particles.[30] The corresponding SAED pattern in the inset figure shows the polycrystallinity of the α-Fe_2O_3 structure.[31]

The cyclic voltammetry (CV) curves of the 73% α-Fe_2O_3/RGO are shown in Fig. 4a. In the first cycle, two cathodic peaks around 0.6 V and 1.6 V represent the gradual reduction of Fe^{3+} to Fe^0 by lithium,[32] corresponding to the conversion reaction:[30,33]

$$Fe_2O_3 + 6Li^+ + 6e^- \rightarrow 2Fe + 3Li_2O.$$

Meanwhile, the anodic peak presented at 1.8 V represents the oxydic reaction from Fe^0 to Fe^{3+}. The reduction peak shifts to 0.7 V in the second cycle because of the irreversible phase transformation in the first cycle which resulted from the decomposition of electrolyte and formation of solid electrolyte interface (SEI).[34] Such an SEI layer usually happens in the LIB anodes in the first cycle.[35,36] After the second cycle, the intensity of the cathodic and anodic peaks remains almost the same, which indicates that the capacity remained unchanged. The cathodic and anodic peaks of the pure Fe_2O_3 (Fig. 4b) appear at 0.6 V and 1.6 V respectively. However the low capacity of the pure Fe_2O_3 makes the peaks inconspicuous. Fe_2O_3 without RGO exhibits a decaying capacity. From the second cycle to the fifth cycle, the area of the curve decreases obviously, indicating the loss of the capacity.

Fig. 5 shows the Nyquist plots of the cells with pure Fe_2O_3 and three α-Fe_2O_3/RGO composites as anodes at a discharge potential of 0.1 V. It is usually considered that the charge-transfer resistance can be signified by the semicircle in the medium-frequency region.[37] Although the materials are combined with carbon black (as a conductive additive), it is obvious that the existence of RGO improves the conductivity of pure Fe_2O_3 a lot. The excellent conductivity of the three α-Fe_2O_3/RGO composites can produce long cycle lifetimes at high rate current density.

The charge–discharge curves of 73% α-Fe_2O_3/RGO at a current density of 100 mA g^{-1} are revealed in Fig. 6a. The initial discharge and charge capacities of the composite are 1578 and 1095 mA h g^{-1}, respectively, resulting in the first coulombic

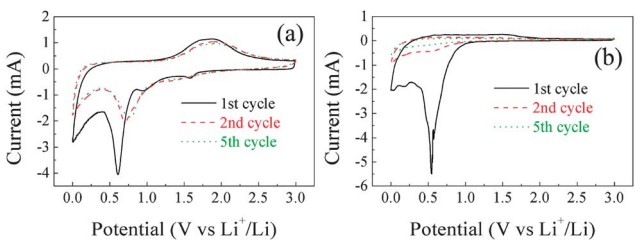

Fig. 4 Cyclic voltammograms of (a) 73% α-Fe_2O_3/RGO and (b) pure α-Fe_2O_3 for the first, second, and fifth cycles at a scan rate of 0.5 mV s^{-1} with a voltage window from 3 to 0 V.

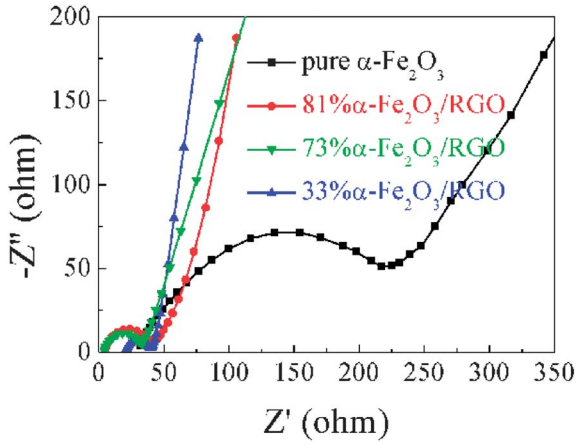

Fig. 5 Nyquist plots of pure α-Fe_2O_3 and three α-Fe_2O_3/RGO composites with different ratios between α-Fe_2O_3 and RGO at a discharge potential of 0.1 V (*vs.* Li/Li^+) from 100 kHz to10 mHz.

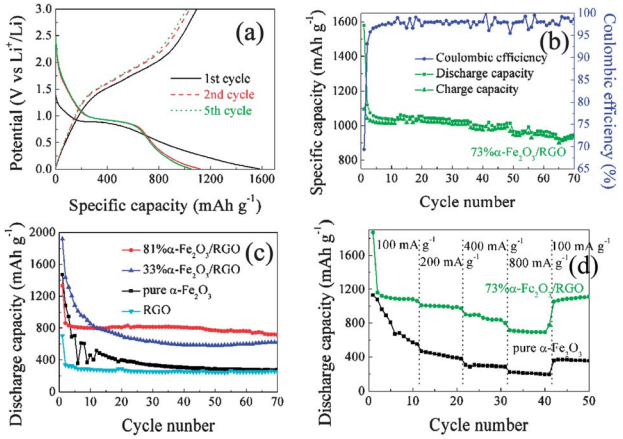

Fig. 6 (a) Lithium insertion/extraction properties of 73% α-Fe_2O_3/RGO. (b) The coulombic efficiency and the cycling performance of 73% α-Fe_2O_3/RGO at a current density of 100 mA g^{-1}. (c) The cycling performance of pure RGO, α-Fe_2O_3, 81% α-Fe_2O_3/RGO and 33% α-Fe_2O_3/RGO at a current density of 100 mA g^{-1}. (d) The discharge performance of α-Fe_2O_3 and 73% α-Fe_2O_3/RGO at various current rates.

efficiency of ~69%. The first discharge curve at ~0.86 V can be attributed to the forming of SEI layers on the graphene surface. After the first cycle, the coulombic efficiency of 73% α-Fe_2O_3/RGO remains above 97%. Fig. 6b shows the cycling performance of 73% α-Fe_2O_3/RGO at 100 mA g^{-1}. After 70 cycles, 73% α-Fe_2O_3/RGO can deliver a reversible capacity of ~950 mA h g^{-1}. The RGO, pure α-Fe_2O_3 particles, 81% α-Fe_2O_3/RGO and 33% α-Fe_2O_3/RGO for comparison show only ~200 mA h g^{-1}, ~250 mA h g^{-1}, ~600 mA h g^{-1} and ~750 mA h g^{-1}, respectively at a current density of 100 mA g^{-1} (Fig. 6c). We reach the conclusion that when the content of α-Fe_2O_3 is 73%, the specific capacity reaches its highest value. Fig. 6d shows the rate capability of α-Fe_2O_3 and 73% α-Fe_2O_3/RGO at different current densities, the specific capacity of 73% α-Fe_2O_3/RGO exceeds that of α-Fe_2O_3 materials. At a current density of 800 mA g^{-1}, the discharge–charge capacity of 73% α-Fe_2O_3/RGO is as high as ~700 mA h g^{-1}, which is much higher than that of α-Fe_2O_3 particles (~200 mA h g^{-1}). As it is known, the conductivity of anode materials plays an important role in electron transmission, especially at high rate current density. By hybridizing with RGO, the impedance of the α-Fe_2O_3/RGO composite (~30 Ω) decreases by one order of magnitude compared to the pure α-Fe_2O_3 particles (~300 Ω). In the charge process, lithium ions diffuse into the anode materials and the higher conductivity facilitates faster ion diffusion, leading to a higher specific capacity. When lithium ions insert into the anode materials, the volume will expand to some degree. The smaller size of the α-Fe_2O_3 particles will tolerate the volume expanding and achieve a higher cycling stability. From Fig. S3a and b† we can see that after cycling 70 times, the α-Fe_2O_3 particles grow slightly to ~40 nm and keep the primary dispersibility.

4 Conclusion

In summary, α-Fe_2O_3/RGO has been synthesized as an anode material for LIBs by a two-step process, the first is the preparation of the $Fe(OH)_3$ sol and then a hydrothermal procedure to synthesize the α-Fe_2O_3/RGO composite. The cycling performance indicates that at 100 mA h g^{-1}, the 73% α-Fe_2O_3/RGO composite can deliver a higher reversible capacity of ~950 mA h g^{-1} after 70 cycles relative to the other two α-Fe_2O_3/RGO composites, notably higher than that of α-Fe_2O_3 materials. Even at 800 mA h g^{-1}, the 73% α-Fe_2O_3/RGO composite maintains a reversible capacity of ~700 mA h g^{-1}. When RGO is introduced to the composite, the reversible capacity is seen to be markedly enhanced. The reasons of the enhancement can mainly be ascribed to two aspects. Firstly, the α-Fe_2O_3/RGO composite with RGO increases the conductivity of the hybrid a lot. Secondly, the small size of the α-Fe_2O_3 particles of 20–30 nm can tolerate the volume expanding and achieve a higher cycling stability. The relationship between the content of RGO in the composites and the reversible capacity is also discussed. We find that when the content of α-Fe_2O_3 reaches 73%, the best reversible capacity is achieved.

Acknowledgements

This work was supported by the National Basic Research Program of China (2012CB932303) and the National Natural Science Foundation of China (Grant no. 51172261).

Notes and references

1 M. Armand and J. M. Tarascon, *Nature*, 2008, **451**, 652–657.
2 R. Mukherjee, A. V. Thomas, A. Krishnamurthy and N. Koratkar, *ACS Nano*, 2012, **6**, 7867–7878.
3 X. Wang, X. Cao, L. Bourgeois, H. Guan, S. Chen, Y. Zhong, D.-M. Tang, H. Li, T. Zhai, L. Li, Y. Bando and D. Golberg, *Adv. Funct. Mater.*, 2012, **22**, 2682–2690.
4 X. Wang, W. Tian, D. Liu, C. Zhi, Y. Bando and D. Golberg, *Nano Energy*, 2013, **2**, 257–267.
5 B. Li, H. Cao, J. Shao, G. Li, M. Qu and G. Yin, *Inorg. Chem.*, 2011, **50**, 1628–1632.

6 H. Wang, L.-F. Cui, Y. Yang, H. S. Casalongue, J. T. Robinson, Y. Liang, Y. Cui and H. Dai, *J. Am. Chem. Soc.*, 2010, **132**, 13978–13980.
7 C.-H. Yim, E. A. Baranova, F. M. Courtel, Y. Abu-Lebdeh and I. J. Davidson, *J. Power Sources*, 2011, **196**, 9731–9736.
8 J. Chen, L. Xu, W. Li and X. Gou, *Adv. Mater.*, 2005, **17**, 582–586.
9 Z. Wang, D. Luan, S. Madhavi, C. Ming Li and X. Wen Lou, *Chem. Commun.*, 2011, **47**, 8061–8063.
10 Y. NuLi, P. Zhang, Z. Guo, P. Munroe and H. Liu, *Electrochim. Acta*, 2008, **53**, 4213–4218.
11 H. S. Kim, Y. Piao, S. H. Kang, T. Hyeon and Y.-E. Sung, *Electrochem. Commun.*, 2010, **12**, 382–385.
12 C. Wu, P. Yin, X. Zhu, C. OuYang and Y. Xie, *J. Phys. Chem. B*, 2006, **110**, 17806–17812.
13 B. Koo, H. Xiong, M. D. Slater, V. B. Prakapenka, M. Balasubramanian, P. Podsiadlo, C. S. Johnson, T. Rajh and E. V. Shevchenko, *Nano Lett.*, 2012, **12**, 2429–2435.
14 J. S. Chen, T. Zhu, X. H. Yang, H. G. Yang and X. W. Lou, *J. Am. Chem. Soc.*, 2010, **132**, 13162–13164.
15 Y. Li, S. Zhu, Q. Liu, J. Gu, Z. Guo, Z. Chen, C. Feng, D. Zhang and W.-J. Moon, *J. Mater. Chem.*, 2012, **22**, 2766–2773.
16 X. Li, X. Meng, J. Liu, D. Geng, Y. Zhang, M. N. Banis, Y. Li, J. Yang, R. Li, X. Sun, M. Cai and M. W. Verbrugge, *Adv. Funct. Mater.*, 2012, **22**, 1647–1654.
17 L. Tian, Q. Zhuang, J. Li, C. Wu, Y. Shi and S. Sun, *Electrochim. Acta*, 2012, **65**, 153–158.
18 H.-C. Tao, L.-Z. Fan, X. Yan and X. Qu, *Electrochim. Acta*, 2012, **69**, 328–333.
19 Y. J. Mai, J. P. Tu, C. D. Gu and X. L. Wang, *J. Power Sources*, 2012, **209**, 1–6.
20 Y. J. Mai, S. J. Shi, D. Zhang, Y. Lu, C. D. Gu and J. P. Tu, *J. Power Sources*, 2012, **204**, 155–161.
21 J. Su, M. Cao, L. Ren and C. Hu, *J. Phys. Chem. C*, 2011, **115**, 14469–14477.
22 F. Xia, X. Hu, Y. Sun, W. Luo and Y. Huang, *Nanoscale*, 2012, **4**, 4707–4711.
23 S. Bai, S. Chen, X. Shen, G. Zhu and G. Wang, *RSC Adv.*, 2012, **2**, 10977–10984.
24 X. Zhu, Y. Zhu, S. Murali, M. D. Stoller and R. S. Ruoff, *ACS Nano*, 2011, **5**, 3333–3338.
25 F. Zhang, H. Cao, D. Yue, J. Zhang and M. Qu, *Inorg. Chem.*, 2012, **51**, 9544–9551.
26 X. Zhou, Y.-X. Yin, L.-J. Wan and Y.-G. Guo, *Chem. Commun.*, 2012, **48**, 2198–2200.
27 C. Wang, D. Li, C. O. Too and G. G. Wallace, *Chem. Mater.*, 2009, **21**, 2604–2606.
28 S. Park and R. S. Ruoff, *Nat. Nanotechnol.*, 2009, **4**, 217–224.
29 W. Chen, S. Li, C. Chen and L. Yan, *Adv. Mater.*, 2011, **23**, 5679–5683.
30 B. Sun, J. Horvat, H. S. Kim, W.-S. Kim, J. Ahn and G. Wang, *J. Phys. Chem. C*, 2010, **114**, 18753–18761.
31 Y. Zou, J. Kan and Y. Wang, *J. Phys. Chem. C*, 2011, **115**, 20747–20753.
32 G.-W. Zhou, J. Wang, P. Gao, X. Yang, Y.-S. He, X.-Z. Liao, J. Yang and Z.-F. Ma, *Ind. Eng. Chem. Res.*, 2013, **52**, 1197–1204.
33 C. Combelles, M. B. Yahia, L. Pedesseau and M.-L. Doublet, *J. Phys. Chem. C*, 2010, **114**, 9518–9527.
34 W. Xiao, Z. Wang, H. Guo, X. Li, J. Wang, S. Huang and L. Gan, *Appl. Surf. Sci.*, 2013, **266**, 148–154.
35 J. Liu, Y. Li, H. Fan, Z. Zhu, J. Jiang, R. Ding, Y. Hu and X. Huang, *Chem. Mater.*, 2010, **22**, 212–217.
36 J. Ma, J. Lian, X. Duan, X. Liu and W. Zheng, *J. Phys. Chem. C*, 2010, **114**, 10671–10676.
37 H. Xiang, K. Zhang, G. Ji, J. Y. Lee, C. Zou, X. Chen and J. Wu, *Carbon*, 2011, **49**, 1787–1796.

